Food Chemistry: X 25 (2025) 102043

Contents lists available at ScienceDirect

Food Chemistry: X

journal homepage: www.sciencedirect.com/journal/food-chemistry-x

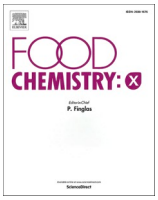

Green hydrothermal approach for the synthesis of carbon quantum dots from waste tea bags for acrylamide detection in drinking water: A fluorescence assay validated by HPLC-PDA analysis

Nikhil Sharma [a], Sweezee Thakur [b], Aarti Bains [c], Gulden Goksen [d], Nemat Ali [e], Mushtaq Ahmad Ansari [e], Anna Kopsacheili [f], Charalampos Proestos [f,*], Prince Chawla [a,*]

[a] Department of Food Technology and Nutrition, School of Agriculture, Lovely Professional University, Phagwara, 144411, India
[b] Department of Food Technology and Processing, School of Health Sciences, Amity University, Punjab, Mohali 140306, India
[c] Department of Microbiology, Lovely Professional University, Phagwara 144411, India
[d] Department of Food Technology, Vocational School of Technical Sciences at Mersin Tarsus Organized Industrial Zone, Tarsus University Mersin, Turkey
[e] Department of Pharmacology and Toxicology, College of Pharmacy, King Saud University, P.O.Box 2457, Riyadh 11451, Saudi Arabia.
[f] Food Chemistry Laboratory, Department of Chemistry, National and Kapodistrian University of Athens, Panepistimiopolis Zographou, 15771 Athens, Greece

ARTICLE INFO

Keywords:
Tea bag
Hydrothermal
Carbon quantum dots
Acrylamide detection
HPLC

ABSTRACT

The study focused on converting tea bag waste into strong fluorescence carbon quantum dots (TBW-CQDs) for the detection of acrylamide in drinking water, antimicrobial activity, and photocatalytic degradation. The TBW-CQDs exhibited blue luminescence and maximum absorbance at 287 nm under UV light and distinctive fluorescence emission and excitation wavelengths at 425 nm and 287 nm, respectively. TBW-CQDs revealed a particle size of 8.12 ± 0.06 nm with a spherical morphology followed by an abundance of 59.29 % carbon and 39.82 % oxygen. For acrylamide extraction from water, the QuEChERS method was established, which exhibited a recovery rate of 97 to 99 %. The fluorescence-based sensor exhibited a low limit of detection of 0.35376 ppm, which was validated by HPLC-PDA (LOD 0.300688 ppm). TBW-CQDs degraded 90.62 % of indigo carmine and 93.19 % of methylene blue under bright sunlight. In conclusion, the fabricated TBW-CQDs provide a promising, cost-effective, and precise approach to acrylamide detection in drinking water.

1. Introduction

Acrylamide (AA), a colorless, odorless crystalline compound with the molecular formula C_3H_5NO, is primarily utilized as a monomer to produce polyacrylamide, which finds widespread applications in industrial processes, particularly in water treatment, agriculture, paper manufacturing, and soil conditioning (Allen, 1978; Fan et al., 2023). Polyacrylamide's role as a flocculant in water purification helps improve water quality, ensuring it is suitable for consumption in the food and beverage industries. However, a significant concern in using polyacrylamide-based filtration membranes is the potential leaching of unreacted AA monomers into treated water, resulting in contamination. This leaching typically occurs when acrylamide is not fully polymerized during membrane manufacturing, allowing residual monomers to dissolve gradually into the water stream (Tepe, 2024).

Several factors influence AA leaching from filtration membranes, including the polymerization process's quality, the membrane's structural integrity, and the specific conditions in water treatment operations, such as pH, temperature, and the presence of other chemicals (Taloor et al., 2024). Since AA is a known carcinogen, its presence in drinking water poses health risks, emphasizing the need for strict quality control during manufacturing and continuous monitoring of treated water to prevent contamination (Gür et al., 2023). The health impacts of AA are well-documented; it is classified by the International Agency for Research on Cancer (IARC) as a probable human carcinogen (Group 2 A), based on animal studies. AA undergoes metabolic conversion to reactive derivatives like glycidamide, which can form DNA adducts, potentially inducing mutations and cellular disruptions leading to cancers, particularly of the kidney, endometrium, and ovaries (Farouk et al., 2021; Yan et al., 2023). Beyond its carcinogenicity, AA exposure also poses genotoxic, neurotoxic, reproductive, and hepatotoxic effects, impacting genes, neurotransmitter levels, and hormone regulation

* Corresponding authors.
E-mail addresses: harpro@chem.uoa.gr (C. Proestos), princefoodtech@gmail.com (P. Chawla).

https://doi.org/10.1016/j.fochx.2024.102043
Received 4 July 2024; Received in revised form 17 November 2024; Accepted 22 November 2024
Available online 29 November 2024

(Gupta et al., 2023). Given these risks, AA contamination in drinking water is a critical public health concern, and ensuring safe levels requires sensitive detection methods (Agbasi et al., 2024; Priya et al., 2018).

Traditional analytical techniques for detecting AA include high-precision methods such as Liquid Chromatography-Mass Spectroscopy (LCMS) (Yazıcı et al., 2023), High-Performance Liquid Chromatography (HPLC) (Feng et al., 2023), Surface Enhanced Raman Spectroscopy (SERS) (Wang et al., 2024), and Gas Chromatography-Mass Spectroscopy (GC-MS) (Aghvami et al., 2023). These methods offer accuracy but are costly, time-consuming, and may require complex instrumentation, limiting their widespread use for routine water quality monitoring. Consequently, there is increasing interest in developing alternative methods that are cost-effective, eco-friendly, and suitable for real-time monitoring of AA in environmental and food samples.

Emerging approaches leverage green and sustainable materials, including carbon quantum dots (CQDs) and biosensors. CQDs are fluorescent nanomaterials with sizes ranging from 1 to 10 nm and exhibit unique properties such as high photostability, water solubility, biocompatibility, and strong, tunable fluorescence. These characteristics make CQDs suitable for various applications, including the targeted drug delivery (Pourmadadi et al., 2024), bioimaging (Atchudan et al., 2021; Molaei, 2024), gene therapy (Zhu et al., 2024), detection of heavy metals (Vyas & Joshi, 2024), toxins (Wei et al., 2020), and pathogens (Hu et al., 2021). Moreover, CQDs have demonstrated significant potential as sustainable alternatives for traditional AA detection methods due to their low toxicity and environmentally friendly production, often derived from food and agricultural waste, which further aligns with sustainable development goals (Pushparaj et al., 2022).

Repurposing food waste to produce CQDs supports the development of cost-effective, high-sensitivity nanosensors and contributes to reducing environmental waste. Among potential CQD sources, tea bag waste (TBW) is particularly promising. Tea, one of the world's most consumed beverages, generates substantial amounts of waste. By 2025, global tea production is projected to reach 8.52 million tons, reflecting a growth rate of 4.9 % annually (Inayat et al., 2023). TBW contains valuable carbon sources and functional groups, such as polyphenols, catechins, lignin, and tannins, which are ideal for CQD synthesis (Osorio et al., 2021; Rajput et al., 2024). These functional groups enable interactions with acrylamide molecules, creating a measurable fluorescence quenching effect suitable for AA detection (Vijeata et al., 2024).

This study explores the use of TBW-derived CQDs for acrylamide detection in drinking water. By utilizing food waste as a carbon source, we address a dual need: creating a sensitive and eco-friendly sensor for AA while promoting sustainable waste management practices. The TBW-CQDs were characterized by their optical and morphological properties, establishing their suitability as a fluorescent nanoprobe. Additionally, the performance of the TBW-CQD sensor was validated through comparison with HPLC-PDA analysis, a traditional AA detection method, ensuring accuracy and reliability. The TBW-CQDs nanoprobe demonstrated considerable potential for real-time monitoring and effective detection of AA in water, offering a practical solution for quality management across various sectors.

2. Material and methodology

2.1. Materials

The research work utilized all chemicals of analytical grade without any further treatment. Acrylamide (CAS No. 79–06-1, purity ≥99 %) was obtained from Central Drug House (P) Ltd. New Delhi, India. β-cyclodextrin (CAS No. 7585-39-9, purity ≥98 %) and syringe filter (0.22 μm) were purchased from Hi-Media Pvt. Ltd. Mumbai, India. Tea waste was sourced specifically from (Lipton black tea bags), ensuring consistency in the raw material used for CQDs synthesis throughout the study. Drinking water was obtained from a local market in Jalandhar, (Punjab, India). QuEChERS Kit (containing 150 mg $MgSO_4$ + 50 mg C-18 Powder +50 mg PSA) was acquired from Thermo Fisher Scientific, USA. A hydrothermal reactor (100 mL) utilized to fabricate CQDs was acquired from Techinstro Industries Nagpur, Maharashtra, India. Acetonitrile (CAS No. 75–05-8, purity ≥99.9 %), n-hexane (CAS No. 110–54-3, purity ≥99 %), Tannic acid (CAS No. 1401-55-4, purity ≥90 %), Gallic acid (CAS No. 149–91-7, purity ≥98 %), Caffeine anhydrous (CAS No. 58–08-2, purity ≥99 %), Quercetin (CAS No. 117–39-5, purity ≥95 %), citric acid (CAS No. 77–92-9, purity ≥99.5 %), Methylene blue (CAS No. 61–73-4, purity ≥82 %), and indigo carmine (CAS No. 860–22-0, purity ≥90 %) were purchased from Loba Chemie Pvt. Ltd. Mumbai, India. All the reagents and samples were prepared in deionized water (CAS No. 7732-18-5) obtained from Loba Chemie Pvt. Ltd. Mumbai, India.

2.2. Proximate analysis of TBW

The proximate composition of TBW was evaluated using the AOAC protocol. Various analytical techniques were utilized to determine the moisture, crude fat, protein, ash, crude fiber, and carbohydrate content of the sample. These parameters were quantified as a percentage.

2.2.1. Moisture content of TBW

The moisture content analysis of the sample was conducted utilizing a hot air oven by following the AOAC guidelines proposed by Dilebo et al. (2023). The initial weight of empty petri dishes (W_1) was recorded, following which 3 g of the sample was deposited into the petri dishes (W_2). Subsequently, the drying was done at 105 °C, facilitating the gradual removal of moisture till a constant weight. Subsequently, the petri dish was placed in a desiccator for cooling and then weighed (W_3). The moisture percentage within the sample was determined using the Eq. (1):

$$\text{Moisture content\%} = \frac{W_2 - W_3}{W_2 - W_1} \times 100 \quad (1)$$

2.2.2. Ash content of TBW

The ash content was determined using the muffle furnace method by following the method given by Mpili et al. (2024). The 1 g of charred TBW powder was incinerated in a crucible within a muffle furnace for 4 h at a temperature of 550 °C. Following the cooling process, the ash was weighed and ash % was determined using the following Eq. (2):

$$\text{Ash (\%)} = \frac{W}{Ws} \times 100 \quad (2)$$

Where, W = Weight of ash residue.
Ws = Weight of sample.

2.2.3. Crude fat content of TBW

The assessment of lipid content was investigated using the Soxhlet method as detailed by Sandeep Kumar Jain et al. (2023). Petroleum ether served as the extraction solvent, with the percentage of lipid determined using the Eq. (3) provided below:

$$\text{Crude Fat (\%)} = \frac{W1}{W2} \times 100 \quad (3)$$

Weight of fat extracted (W1) = Weight of Round bottom flask (RBF) after extraction – weight of empty RBF.
W2 = Weight of Sample.

2.2.4. Protein content of TBW

The quantification of total nitrogen in the sample utilizing by the CLASSIC DX *VA* TS, Pelican Equipment, India (Zafar et al., 2023). A conversion factor of 6.5, relating nitrogen to protein content, was applied for protein determination in the sample (Eq. 4).

$$\text{Protein\%} = \frac{N \times V \times 6.25}{Ws} \times 100 \quad (4)$$

where, V = volume of the sulfuric acid.
N = normality of the acid.
Ws = weight of the sample.

2.2.5. Crude fiber of TBW

The crude fiber was done according to Olugbuyi et al. (2024). The 1 g TBW sample (W) underwent a digestion process for 30 min in a water bath containing 0.255 M sulfuric acid. Following cooling, the digested sample was filtered, and the residue was rinsed 2–3 times with distilled water. Subsequently, the residue was subjected to a 30 min boiling process with 0.313 N sodium hydroxide, followed by washing with distilled water. The resulting residue was then transferred to a petri dish (W_1) and heated in an oven at 110 °C for 2 h. After cooling, the weight was recorded (W_2). The moisture-free residue was further placed in a muffle furnace for 6 h, and the weight was recorded after cooling (W_3). The weight of the empty crucible is denoted as W_4. The crude fiber (%) was estimated using the Eq. (5):

$$\text{Crude fiber (\%)} = \frac{W_3 - W_4}{W} \times 100 \quad (5)$$

2.2.6. Total carbohydrate of TBW

The carbohydrate content in TBW was determined using the difference method. The rest of the other components such as protein, crude fat, ash, and moisture are subtracted from the total weight of the food matrices in the Eq. (6).

$$\text{Total Carbohydrate} = 100\text{–}(\text{Protein} + \text{crude fat} + \text{ash} + \text{moisture}) \quad (6)$$

2.3. Fabrication of CQDs from tea bag waste

CQDs were fabricated from tea bag waste using a simple hydrothermal method according to Irmania et al. (2020) with certain modifications. Initially waste tea bag was dried, ground, and finely powdered. Dissolve 200 mg of waste tea bag powder in 90 mL of deionized water. The solution is transferred to a 100 mL Teflon-lined stainless steel hydrothermal reactor and kept at 180 °C for 9 h. The yellow suspension is further centrifuged at 5000 rpm for 20 min and purified using a 3KDa dialysis membrane. The fabricated TBW-CQDs underwent filtration using a 0.45 μm syringe filter. The transparent yellow solution (TBW-CQDs), exhibiting remarkable fluorescent properties was obtained and finally, stored at refrigeration condition (At 4 °C) till further characterization.

2.4. Characterization of TBW-CQDs

The characterization of waste tea bags derived from carbon quantum dots was carried out using a range of analytical techniques such as UV–visible spectroscopy, Particle size analyzer and zeta potential, TEM, FTIR, DSC, and Fluorescence spectroscopy.

2.4.1. UV–visible spectroscopy of TBW-CQD

The confirmation of TBW-CQDs was achieved through the utilization of UV in the visible spectrum according to Kasinathan et al. (2022). The UV–visible spectrophotometer (Thermo Scientific NanoDrop Lite UV Visible spectrophotometer, Waltham, USA) was used. To prepare the sample, 100 μL was diluted in 2.9 mL of deionized water. A quartz cuvette with a capacity of 4 mL was filled with the diluted sample, while a second cuvette was filled with deionized water as a control. The experiment was conducted at ambient conditions, covering a spectral range from 800 nm to 200 nm. Subsequently, the spectra were monitored across various wavelengths using a computer equipped with UV-probe software.

2.4.2. Particle size analysis (PSA) and zeta potential (ZP) of TBW-CQDs

The PSA and ZP of TBW-CQDs were determined using by Mastersizer (3000+ Lab, Malvern Panaltyical Ltd., UK) according to method of Marouzi et al., (2021). The sample preparation, 500 μL of TBW-CQDs were mixed with deionized water using an Ultrasonic homogenizer (HD 4100 SONOPLUS, Bandelin Electronic GmbH & Co. KG., Germany). Subsequently, the prepared sample underwent PSA using a 4 mL quartz cuvette.

2.4.3. Morphological and elemental characteristics of TBW-CQDs

The internal morphology and elemental analysis of TBW-CQD were analyzed by HR-TEM (Thermo scientific Talos™ F200X G2), following the method outlined by Sistani and Shekarchizadeh (2021). The sample was analyzed with operating at 20 mV. Additionally, HR-TEM was equipped with energy dispersive spectroscopy (EDS) from Thermo Scientific at 10 mv and was subjected to further study. The 10 μL of TBW-CQD sample was placed over the copper grid, following the sputtering process at the voltage of 30 mA for 2 min. The images were recorded with the help of Thermo Scientific Velox software at different magnifications.

2.4.4. Fourier transform infrared spectroscopy (FTIR) of TBW-CQDs

The functional groups present on the surface of fabricated carbon nanoparticles were analyzed using FTIR (Paragon 1000, Perkin Elmer, Spectrum Two, USA) ((Zhang et al., 2023). This analysis was performed under ambient temperature and working in the mid-infrared region spectrum range i.e. 4000–400 cm^{-1}. This instrument comprises a diamond crystal cell Attenuated total reference (ATR) operated at 0.5 cm^{-1} resolution. The 200 mg of KBr powder was mixed with 20 μL TBW-CQD and further loaded onto the sheet. The FTIR spectra of the samples were generated in terms of transmittance and wavenumber.

2.4.5. Thermal properties of TBW-CQDs

Thermal properties of TBW-CQDs were analyzed by Differential scanning calorimetry (DSC) (Perkin Elmer 6000, Norwalk, USA) described method by Thakur, Bains, Kumar, et al. (2024). This analysis was conducted under a controlled atmosphere of a nitrogen gas (N_2) with temperatures ranging from 25 °C to 350 °C at a constant scanning rate of 10 °C/min, using a bare aluminum (Al) pan as reference. This DSC analysis was utilized to identify parameters such as set temperature, onset temperature, melting peak temperature, and melting enthalpy.

2.4.6. Fluorescence spectroscopy (FS) of TBW-CQDs

The fluorescence analysis was conducted in accordance with Alamdari et al. (2023) using the Fluorescence Spectrophotometer (F-7000 Hitachi High-tech Corporation, Japan) featuring a 1.0 cm quartz cuvette. The excitation wavelength of 287 nm was applied to the sample with a scanning rate of 10 nm/min across the 800–350 nm range. A 3.5 mL cuvette with a path length of 3.5 cm was used for the synthesized TBW-CQD sample, resulting in spectrum generation. The spectrum was recorded and analyzed on a computer using the software Spectrum FLR version 1.1 at different wavelengths.

2.4.7. Atomic force microscopy (AFM) of TBW-CQDs

The surface topography of tea-derived carbon dots was recorded by AFM (Asylum MFP-3D, Oxford, UK) (Kalpana et al., 2023). A single drop of TBW-CQDs was added to deionized water, and the resulting mixture was spread onto a silicon wafer. Subsequently, the wafer underwent drying at 28 °C, with a scanning rate of 0.5–1 line.

2.5. Quantum yield of TBW-CQDs

The quantum yield of the TBW-CQDs was measured according to Anpalagan et al. (2024) utilizing the Eq. (7):

$$\Phi = \{\Phi r \times I/Ir \times Ar/A \times \eta/\eta r\} \quad (7)$$

In this equation, Φ signifies the comparative quantum yield of the CQDs relative to that of quinine sulfate, which has a concentration of 0.1 mg/L when dissolved in 0.1 M H_2SO_4 and is used as the reference (Φr) with an excitation wavelength of 360 nm. "I" stands for the total emission intensity derived from the emission spectrum with a 360 nm excitation. "A" is the UV–visible light absorbance at 360 nm, which is kept under 0.05 in the 10 mm quartz cell to avoid re-absorption effects. The refractive index of the solvent (η) was noted as 1.33.

2.6. Detection of acrylamide using TBW-CQDs

The detection of acrylamide was undertaken with the determination of TBW-CQDs fabricated from waste tea bags by the dilution of CQDs into deionized water (Wei et al., 2021). Different concentrations of acrylamide (0.5, 1.0, 1.5, 3.0, 5.0, and 10.0 ppm) were incorporated into 3.0 mL of TBW-CQDs and incubated for 30 min. Afterward, the photoluminescence (PL) emission spectrum of TBW-CQDs containing different concentrations of acrylamide was recorded and analyzed. The change/shift in the PL spectrum of TBW-CQDs due to the presence of variable concentrations of acrylamide or fluorescence intensity of TBW-CQDs along with different concentrations of acrylamide tends to make an impact on the PL spectrum.

2.7. Selectivity of TBW-CQDs for acrylamide detection

The sensitivity, precision, and selectivity of tea bag-derived carbon dots were investigated by employing interference of tannic acid, gallic acid, caffeine, and quercetin (John et al., 2024). These chemical containments were incorporated into the solution, and the resulting solution underwent fluorescence sensing for evaluation. The shift in fluorescence intensity and wavelength of carbon dots were investigated in the context of various chemicals mentioned before (reaction time: 30 min, and reaction temperature 25 °C). The evaluating the interaction among the TBW-CQD with these different interference substances assists in determining the specificity and sensitivity of the fluorescent nanoprobe throughout the wide range of the analytes.

2.8. Pretreatment of drinking water sample

Drinking water bottles were purchased from a market in Jalandhar, Punjab, India. Firstly 10 g of sample was taken along with 10 mL of acetonitrile and placed into a 50 mL centrifuge tube. Following that 4 *g* of $MgSO_4$ and 1 g of NaCl were added into the tube. Centrifuge sample 7000 rpm for 15 min to separate acrylamide from food matrix and keep the supernatant for further analysis. QuChERS kit containing 150 mg of $MgSO_4$, 25 mg of primary secondary amines, and 25 mg of C-18 powder was added to 1 mL aliquot. Following that, emission spectra were recorded using a fluorescence spectrophotometer with a 290 nm excitation wavelength. The LOD was determined with the procedure outlined by Casanova et al. (2023) as dividing 3 times the standard deviation(SD) of the calibration curve's intercept by the slopes of the curve.

2.9. Analysis of food sample

In the analysis of drinking water, two analytical approaches were employed TBW-CQDs fluorescence sensor and HPLC-PDA. An aliquot of 20 μL isolated from a drinking water sample was directly incorporated into fabricated TBW-CQDs. The shift in the fluorescence intensity of TBW-CQD was used as the confirmation for the presence of acrylamide in our sample (drinking water).

Determination of acrylamide in food samples was done with two methods i.e. High-Performance Liquid Chromatography and Fluorescence sensing with assistance with TBW-CQDs. The gradient flow of water/acetonitrile (97:3) was carried out for the analysis with a flow rate of 0.7 mL/min and the injected sample volume was 20 μL. The wavelength of the PDA detector was maintained at 202 nm. The acrylamide was eluted at 3.97 min. The isocratic flow of water/acetonitrile (20:80) was utilized for the cleaning of the column. The total run time was 40 min. The determination of acrylamide in the food sample was based on the spectrum of the sample along with the retention time.

2.10. Antimicrobial properties of TBW-CQDs

The effectiveness of the fabricated fluorescent carbon quantum dots (CQDs) against *Escherichia coli, Pseudomonas aeruginosa,* and, *Staphylococcus aureus*, was assessed using the well diffusion method as given by Pandiyan et al. (2020). To ensure sterility, both the petri dish and the samples underwent sterilization at 120 °C for 30 min before the antimicrobial activity testing. Fresh bacterial inoculums were evenly spread across the surface of the nutrient agar medium using a sterile cotton swab. The preparation of the testing solution entailed the combination of the tea-derived carbon dots stock solution with sterile Milli-Q water. Initially, the TBW-CQDs were dissolved in sterile distilled water to prepare a stock solution. Subsequently, wells were filled with 0.01 μg/mL of the tea derived-carbon quantum dots solution and incubated for 24 h at 37 °C. The resulting inhibition zones (measured in mm) formed in the petri dish were then observed and recorded. Furthermore, the minimum inhibitory concentration (MIC) and minimum bactericidal concentration (MBC) were assessed using the broth microdilution method. the plates were incubated at 37 ℃ for 24 h, with the MICidentified as the lowest concentration of TBW-CQDs that visibly inhibited bacterial growth. The MBC was established by subculturing the contents from the MIC wells onto MHA plates.

2.11. Photocatalytic dye degradation

The effectiveness of tea-derived carbon dots in catalytic degradation of indigo carmine (10 ppm) and methylene blue (10 ppm) dyes was evaluated following the approach by Abu-Melha (2024) under natural sunlight. To establish absorption-desorption equilibrium, the TBW-CQDs-dye solution underwent constant magnetic stirring at 200 rpm in darkness for 20–30 min. In summary, 100 mL of dye solution and 10 mL of TBW-CQDs were mixed in a conical flask and exposed to natural sunlight with constant stirring. During the analysis, 2 mL aliquots were withdrawn at specified intervals (15, 30, 45, 60, 75, 90, 100, and 120 min) and centrifuged at 10000 rpm for 15 min. Following centrifugation, the dye concentration was determined using a Thermo Scientific NanoDrop Lite UV Visible spectrophotometer based on absorption spectra. The calculation of dye degradation efficiency employed the following equation.

$$\text{Degradation efficiency } (\%) = (C_I – C_F) \times 100.$$

where C_I and C_F represent the initial and final dye concentrations (mg/L) of the dye-CQDs complex at time 0 and t respectively.

2.12. Statistical analysis

The trials were carried out in triplicate, and the standard error of the mean was calculated using Microsoft Excel 365. The critical difference (CD value) was used to compare means in Microsoft Excel 365 (Microsoft Corp., Redmond, WA) with the help of the data analysis tool. The software was used to determine standard deviation and average values. For statistical analyses, the significance level was set at $p < 0.05$. OriginPro 8.5, (OriginLab Co., Northampton, MA, USA) was used to generate all the figures. Statistical analysis was performed using ANOVA (Analysis of Variance) to evaluate the significance of the results, with a threshold of $p < 0.05$ considered statistically significant.

3. Results and discussion

3.1. Proximate analysis of TBW

The nutritional breakdown of tea bag waste was determined. The moisture content of the TBW was 71.37 ± 0.21 %. Total ash content signifies the overall mineral content in food, and across TBW, contains ash content of approximately 1.62 ± 0.02 %. The estimation indicated protein level in TBW was 15.19 ± 0.17 %. The protein content in spent black tea is higher due to the retention of residual tea leaves and particulate matter after brewing, leading to a concentration of nutrients in the spent leaves. Tea contains lipids including triglycerides, fatty acids, phospholipids, and sterols, although present in relatively less proportions. The crude fat percentage in TBW was approximately 1.25 ± 0.01 %. The crude fiber content was 5.91 ± 0.06 %.

3.2. 3.2 Synthesis mechanism of TBW-CQDs

In this study, the tea bag waste as a carbon source was utilized for tailoring TBW-CQDs. These tea bags contain several organic compounds such as lignin, hemicellulose, cellulose, and polyphenols as major catechins i.e. Epigallocatechins-3-gallate, Epicatechin-3-gallate, Epigallocatechin, and Epicatechin. Polyphenols were selected for the fabrication of TBW-CQDs owing to their hydrophobic backbone along with hydrophilic sidechains comprising -OH and -COOH groups (Inayat et al., 2023). Furthermore, these carbon dots derived from tea waste showcased negligible toxicity, eco-friendliness, cost-effectiveness, optical stability, and strong fluorescence properties. This study utilized tea waste for the synthesis of CQDs due to the presence of abundant carbon, hydrogen, and oxygen in organic molecules. This study utilized different time and temperature combinations ranging from 140 °C to 180 °C for 3 to 9 h. During the fabrication process of TBW-CQDs, deionized water is utilized as a reaction solvent, thus facilitating the detection of AA. In the hydrothermal treatment, the carbon source undergoes several controlled reactions that result in oxidation leading to an increase in the quantum yield. These reactions take place at high temperatures and pressure that results in interaction among molecules of water and carbon source (Zhong et al., 2023). In a Teflon-lined stainless steel hydrothermal reactor, the reaction medium experiences a pressure increase as the temperature rises. The increase in the pressures results in the breakdown of water molecules into hydroxyl ions (OH^-) and hydrogen ions (H^+), resulting in repulsion between carbon layers and hydrogen bond formation (Aygun et al., 2024).

The final time and temperature combination was selected based on the blue color of CQDs under UV light. In the presence of UV light carbon dots exhibit strong blue luminescence without any treatment. During the reaction, a reduction in particle size resulted in strong fluorescence emission of TBW-CQDs. Due to pressure generated during the treatment carbon nanoparticles underwent carbonization and removal of water. The color changes of TBW-CQD from dark brown to light brown signify the fabrication of carbon dots along with a change in surface morphology. The incorporation of hydrophilic components into TBW-CQDs' structure facilitated their efficient dispersion in aqueous solutions, making them viable for utilization in applications such as analyte detection, wastewater purification, and dye degradation (Kuppusamy et al., 2024). Consequently, the hydroxyl ion interacts with the alcohol group within the polyphenol and lignin structure resulting in the elimination of hydrogen and formation of carbonyl moiety. Furthermore, water molecule promotes the disruption in π-π carbon bond leading to the development of hydroxyl and carboxyl groups on the surface of TBW-CQDs. The spontaneous arrangement of fabricated CQDs is impacted by hydrogen bonding, mainly associated with atoms such as hydrogen and oxygen. The reduction in the distance between -OH groups resulted in the development of the O-OH bond. Due to the availability of electrons on the H atom for covalent bonding to any O atom leading to hydrogen bonding and promotes spontaneous arrangement of the TBW-CQDs during the hydrothermal approach, facilitating the fabrication of carbon nanoparticles.

3.3. Characterization of TBW-CQDs

3.3.1. Optical properties of TBW-CQDs

Fig. 1A illustrates the UV–visible absorption spectra of the TBW-CQDs at a distinctive peak of 287 nm. This absorption peak is attributed to π-π* transition due to aromatic sp^2 hybridization in the TBW-CQDs solution. The CQDs fabricated from tea bag waste exhibit strong blue luminescence under UV light and light brown color in daylight. These CQDs display an excitation wavelength at 287 nm and emission wavelength at 425 nm by fluorescence spectroscopy as depicted in Fig. 1B. These fluorescence properties of the fabricated TBW-CQDs depend upon several factors such as quantum effects, emissive traps, and surface area. The results were supported by Atchudan et al. (2021), which outlined the UV–visible spectra of CQDs derived from the banana peel, observing the peak at 277 nm and 322 nm. This study reported the increase in fluorescence intensity of CQDs up to 355 nm and further decreased afterward. Furthermore, the emission wavelength of these carbon dots demonstrated a redshift.

3.3.2. PSA and ZP of TBW-CQDs

The particle size of TBW-CQDs was depicted in Fig. 1C revealed the average size of carbon dots was 8.12 ± 0.06 nm along with a polydispersity index of 0.3 ± 0.07. There were several factors influencing the particle size of C-QD derived from tea bag waste. The particle size below 10 nm and PDI (Polydispersity index) below 0.4 is appropriate for further analysis. The zeta potential on the surface of TBW-CQD was represented in Fig. 1D. The observed negative surface charge of −13.8 mV confirmed the stable aqueous solution. The noted results confirmed the stability of TBW-CQDs to avoid aggregation among the particles due to the electrostatic interaction of the molecules. These results are well supported by the findings of Hu et al. (2021), who outlined the negative surface charge of −31.2 mV for CQDs derived from orange peel for the detection of *Escherichia coli* in milk samples.

3.3.3. Molecular characterization of TBW-CQDs

The FTIR spectrum of TBW-CQDs was depicted in Fig. 1E, in which different functional groups were identified by utilizing FT-IR spectroscopy. The TBW-CQDs showed a distinctive peak of 3334.92 cm^{-1} associating with the -OH functional group. This recommends the hydrothermal cleavage of the crystalline linkage produced by oxygen in tea bags resulting in highly water-soluble carbon dots. A sharp peak was attained at 2989.99 cm^{-1} indicating the C—H stretching of the alkyl group. A distinctive peak was recorded at 2360.81 cm^{-1} due to the presence of acetylene group or double bonds. The IR spectra at 1636.38 cm^{-1} were attributed to the stretching vibration of the C═O group. The peaks at 1406.32 cm^{-1} were associated with the bending vibration of C—H alkanes and the stretching vibration of the C═C aromatic group., while the peak at 1056 cm^{-1} corresponds to the ether group (C—O). Furthermore, the absorption peak at 589.64 cm^{-1} corresponded to the C—O bond and epoxy groups highlighting the different surface functional groups present in the TBW-CQDs. These findings align with a study by Tungare et al. (2020), where CQDs fabricated from *Phoenix dactylifera* were discovered in various functional groups such as -OH, -COOH, and C—O. This study highlighted the presence of C—O, and C-N-C on the surface of carbon dots.

3.3.4. Morphological and elemental characterization of TBW-CQDs

The HR-TEM micrographs of TBW-CQDs, exploring the structure and internal morphology of the tailored TBW-CQDs were indicated in Fig. 1F. HR-TEM was employed to analyze the fabricated TBW-CQDs at high temperatures, monitoring the aggregation of small particles to produce larger ones. The elemental composition was revealed by energy-dispersive X-ray spectroscopy coupled with HR-TEM resulting in

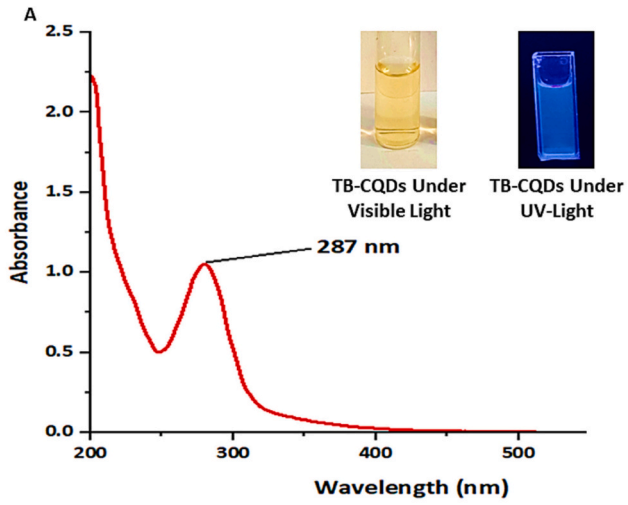

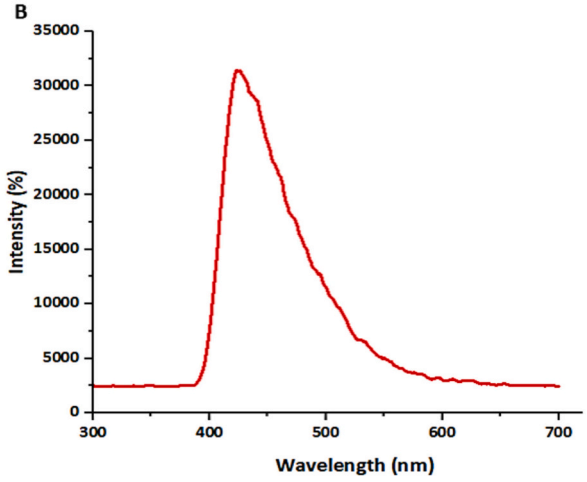

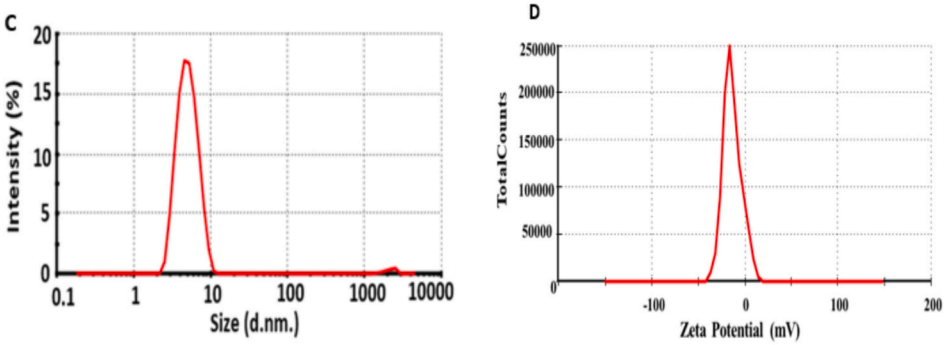

Fig. 1. Characterization of TB-CQDs (Tea bag waste-derived Carbon quantum dots). (A) UV–visible spectrum; (B) fluorescence emission spectra; (C) average particle size (D) zeta potential; (E) Fourier transform infrared spectroscopy; (F) high-resolution transmission electron microscopy; (G) energy dispersive X-ray spectroscopy mapping; (H) differential scanning calorimetry; and (I) Atomic force microscopy. Data are presented as means±SD ($n = 3$).

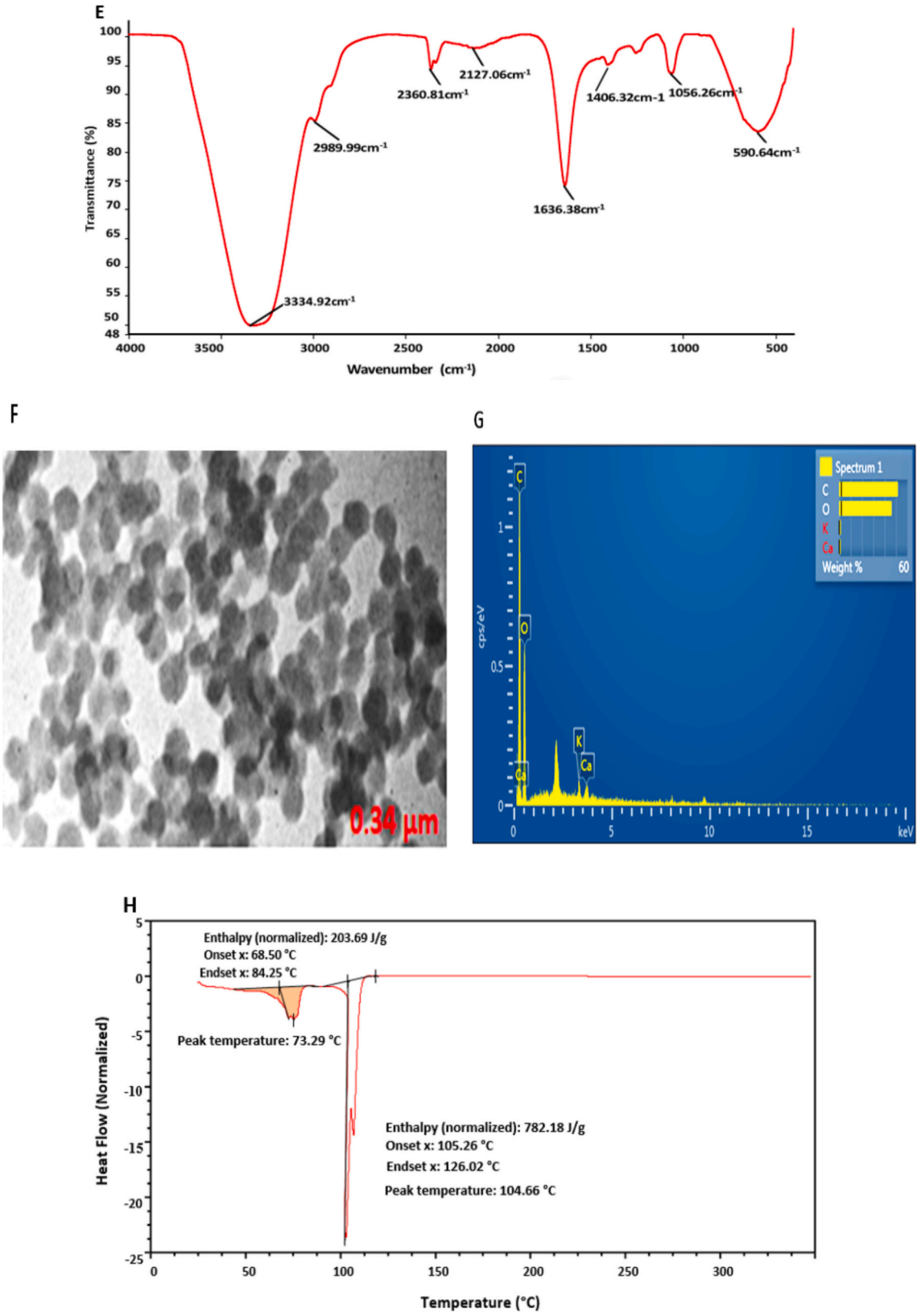

Fig. 1. (*continued*).

a composition of 59.29 % C, 39.82 % O, 0.46 % K, and 0.43 % Ca by total weight. These results also validated the metal-free TB-CQDs sample. As depicted in Fig. 1G, TBW-CQD exhibited uniform spherical particles ranging from 1 to 9 nm, with an average size of 3.43 nm. TBW-CQDs showcased monodisperse size regardless of being light in weight. Our results are well aligned with the findings of Baslak et al. (2023), who fabricated CQD from fermented tea and attained the monodisperse size of 10.0 nm with a spherical shape.

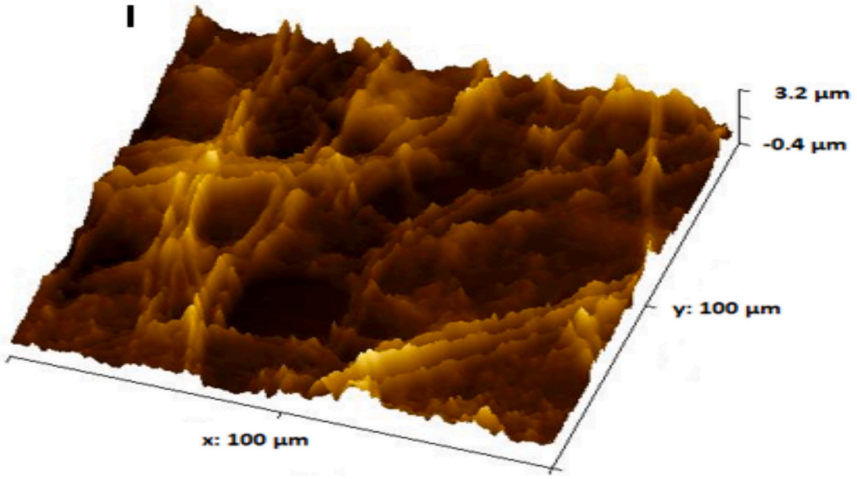

Fig. 1. (*continued*).

3.3.5. Thermal properties of TBW-CQDs

The thermal properties of TBW-CQDs were shown in Fig. 1H. The Differential scanning calorimetry (DSC) curve revealed the removal of water, illustrated by exothermic reaction with an enthalpy of 203.69 J/g at temperatures of 68.50 °C and 84.25 °C. The TBW-CQDs thermally decomposed at 101.12 °C along with an enthalpy of 203.69 J/g. The release of organic content from carbon sources occurs at a temperature of 101. 97 °C.The breakdown of the bonds among organic components results in energy release. Consequently, this leads to the oxidative decomposition. The TBW-CQDs experienced oxidative degradation in the second step at onset and endset temperatures of 105.26 °C and 126.02 °C respectively. Also, mass loss was monitored throughout the second stage. The outcomes were in line with the results of Thakur, Bains, Inbaraj, et al. (2024), revealing two notable endothermic peaks of *Phaseolus vulgaris*-derived CQDs during the heating. The initial peak attributed at 79.74 °C highlights the breakdown of H-bonds between carbon atoms. Then, another peak at 103.08 °C indicates the evaporation of the liquid part (water). Moreover, the absence of a degradation peak below 100 °C illustrates the expectational thermal stability of *Phaseolus vulgaris*-derived CQDs.

3.3.6. Atomic force microscopy of TBW-CQDs

The homogeneity and uniform aggregation of TBW-CQD particles are displayed in Fig. 1I. AFM revealed the roughness and surface topography of the tea-derived carbon dots. These images were utilized to determine the interaction surface force among the probe tip and TBW-CQDs. The shape and height of TBW-CQDs were analyzed through these images resulting in a height of 3.2 µm within a 25 × 25 µm scale. Hence, the TBW-CQDs particle comprises 1 to 3 layers, supporting previous studies. The CQD structure primarily consists of hydrogen and oxygen groups. These outcomes are aligned with the study of Kechagias et al. (2023), who fabricated carbon nanoparticles from Greek crayfish food waste for the strawberry preservation. This study revealed the presence of 1–4 layers.

3.4. Quantum yield of TBW-CQDs

The fluorescence emission spectrum of the TBW-CQDs and reference were recorded with an excitation wavelength of 360 nm. The quantum yield of TBW-CQDs was found to be 40.86 %. This suggests efficient light emission properties, which could be valuable in various applications such as fluorescence imaging, biosensors, and photocatalysis. Our outcomes are well supported by the highlights of Salman (2024), who synthesized sucrose and urea-derived CQDs for the detection of Allura red dye in food beverages. This study reported a high quantum yield of 36 %.

3.5. Selective sensing of acrylamide

The utilization of TBW-CQDs in the detection of acrylamide was depicted in Fig. 2. The interaction between TBW-CQDs and acrylamide was explored based on the shift in fluorescence intensity of TBW-CQDs. The emission spectra of TBW-CQDs were recorded with an excitation and emission wavelength of 287 nm and 425 nm respectively. Moreover, different concentration of acrylamide (0.5 to 10 ppm) was incorporated into TBW-CQDs to explore the stability and sensitivity. The shift in the wavelength of TBW-CQDs confirms the presence of acrylamide, which resulted in a decrease in the emission intensity of TBW-CQDs. AA interacts with TBW-CQDs by altering surface states and causing charge transfer. These interactions modify the electronic structure, increasing the band gap, which leads to higher energy transitions and shorter emission wavelengths (blue shift). This effect is due to changes in energy levels and electron density distribution within the TBW-CQDs. The initial intensity without AA is denoted with the F_0 and the fluorescence intensity in the presence of AA by F. The linear regression equation was $(F_0 - F/F_0) = 0.0381\times + 0.0067$, where x was the concentration of AA.

As the concentration of acrylamide increases, the fluorescence

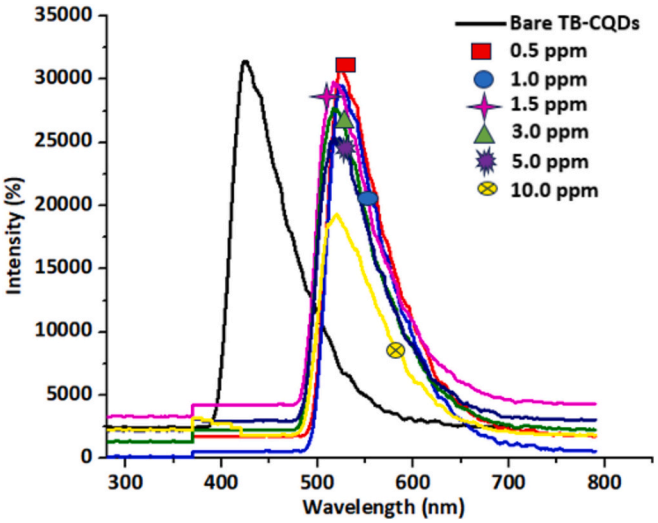

Fig. 2. Fluorescence emission spectra of TB-CQDs were recorded at different concentrations of acrylamide ranging from 0.5 ppm to 10.0 ppm. Data are presented as means ± SD (n = 3).

intensity decreases, and the fluorescence wavelength shifts to 520 nm. The linear range covers concentrations from 0.5 ppm to 10 ppm, exhibiting a high correlation coefficient (R^2 = 0.9991). The limit of detection (LOD) was calculated by LOD = 3*Standard Deviation/ slope of the calibration curve. Notably, the LOD of the fabricated fluorescent sensor was around 0.35376 ppm, owing to their good reliability and sensitivity.

The results of the developed fluorescent sensors were validated with the HPLC-PDA analysis. The different concentration of AA (0.5, 1.0, 1.5, 3.0, 5.0, and 10.0 ppm) was incorporated into the sample and injected into the instrument. The analysis was conducted using a mixture of water and acetonitrile in a ratio of (97:3), with a flow rate of 0.7 mL/min. The elution of AA occurred within the timeframe of 3.87 min as displayed in Fig. 3 (overlay chromatogram). The linear regression equation was Area = 350,760×-60,769, where x was the concentration of AA as depicted in the calibration curve. This analysis provided us with the correlation coefficient R^2 = 0.9994 and revealed the LOD was around 0.300688 ppm. This clearly illustrated the results from the developed TBW-CQDs were close to the HPLC-PDA, which validated our results.

3.6. Acrylamide interference study

The selectivity of TBW-CQDs towards acrylamide is represented in Fig. 4. The selectivity of TBW-CQDs towards acrylamide was explored by mixing with tannic acid, gallic acid, caffeine, and quercetin. There was no particular change in the fluorescence intensity of the solution in contrast to the TBW-CQDs solution as illustrated in Fig. 2C. However, acrylamide was incorporated into an aqueous solution of TBW-CQDs, and a significant decrease and shift in fluorescence intensity was observed. This leads to the change in the emission spectra of TBW-CQDs, which serves as confirmation of acrylamide presence and selectively of TBW-CQDs. Moreover, TBW-CQDs was incorporated into the mixture comprising all non-quenching analytes, and fluorescence intensity was recorded. Our results are supported by the study of Wei et al. (2020) who utilized sucrose, L-aspartic acid, and Ca^{2+} as interference agents in the detection of acrylamide using citric acid-derived CQDs.

3.7. Acrylamide sensing in drinking water

The determination of AA in actual food samples is summarized in Table 1. During the analytical procedure, the aqueous extract of the sample is filtered through a 0.45 μm syringe filter to remove the large particle. Subsequently, different concentrations of the AA (15, 25, and 35 ppm) were deliberately added to pre-treated drinking water samples. The outcomes showcased exceptional accuracy and consistent recovery rates ranging from 98 % to 99 % for TBW-CQDs. However, HPLC-PDA provides a recovery rate of 97 to 98 %, which highlights the precision and accuracy of fabricated fluorescent nanoprobes. These results are consistent with the research conducted by Wei et al. (2020), which detected acrylamide in potato chips by employing citric acid-derived CQD, attaining a (LOD) of 2.6 × 10^{-7} M. Fig. 5 illustrates the increase in the particle size of TBW-CQDs in the presence of acrylamide. The results obtained from PSA and HR-TEM revealed a significant increase in particle size of carbon dots up to 270.72 ± 31 nm and 50.96 ± 14 μm respectively. This increase in particle size is attributed to the aggregation of carbon nanoparticles.

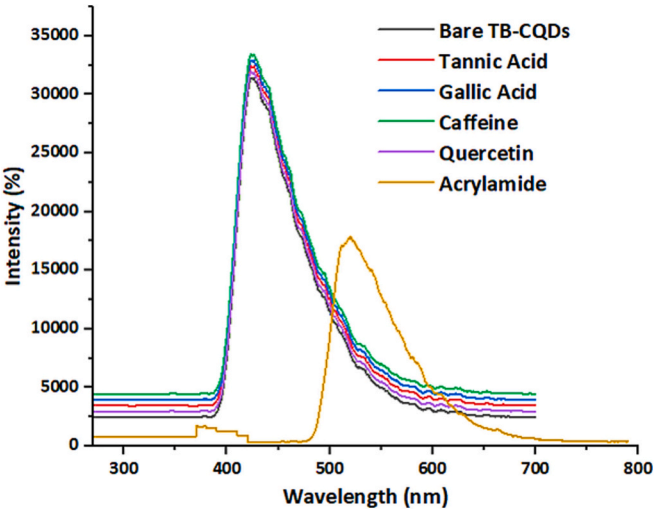

Fig. 4. Effects of interferents on the fluorescence performance of TB-CQDs. Data are presented as means ± SD (n = 3).

3.8. Antimicrobial properties of TBW-CQDs

The evaluation of the antibacterial attributes of TBW-CQDs demonstrates their efficacy against both Gram-positive and Gram-negative bacterial strains, as illustrated in Fig. 6A. In comparison to the chloramphenicol (positive control), which exhibited a notably larger zone of inhibition (26.02 ± 0.47 mm), LW-CQDs displayed a significantly

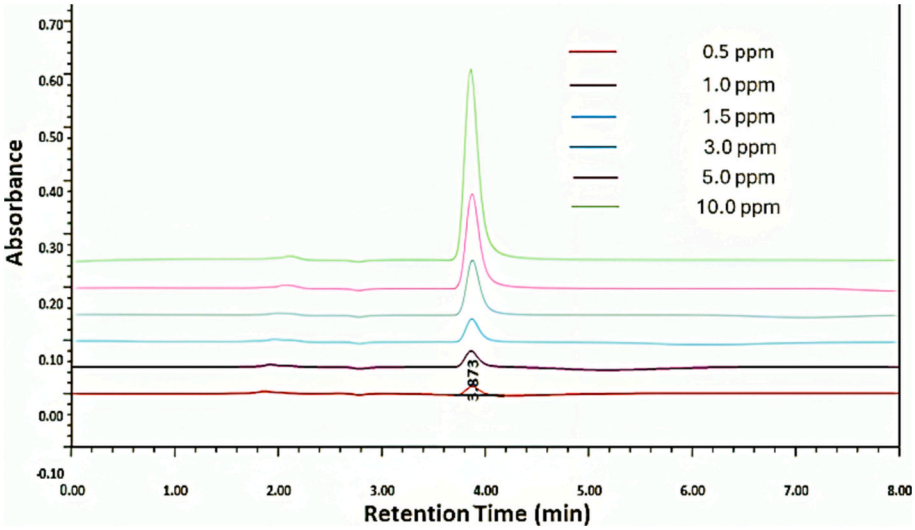

Fig. 3. Overlay Chromatogram of a drinking water sample spiked with various concentrations of acrylamide. Data are presented as means ± SD (n = 3).

Table 1
Recovery of Acrylamide in real food sample.

Sample	TB-CQDs				HPLC-PDA			
	Found Value (ppm)	**Spiked Value (ppm)**	**Observed value after spiking (ppm)**	**Recovery (%)**	**Found Value (ppm)**	**Spiked Value (ppm)**	**Observed value after spiking (ppm)**	**Recovery (%)**
Drinking Water	0	15	14.84 ± 0.26	98.93 ± 0.47[b]	0	15	14.63 ± 0.33	97.53 ± 0.39[a]
	0	25	24.39 ± 0.39	97.56 ± 0.52[a]	0	25	24.57 ± 0.41	98.28 ± 0.42[b]
	0	35	34.68 ± 0.42	99.08 ± 0.61[b]	0	35	34.47 ± 0.19	98.48 ± 0.28[a]

[a]Real food sample is drinking water. Data were expressed as mean ± standard deviation. Mean values within a row with different lowercase superscripts (a-b) are significantly different ($p < 0.05$) from each other based on Duncan's multiple range test.

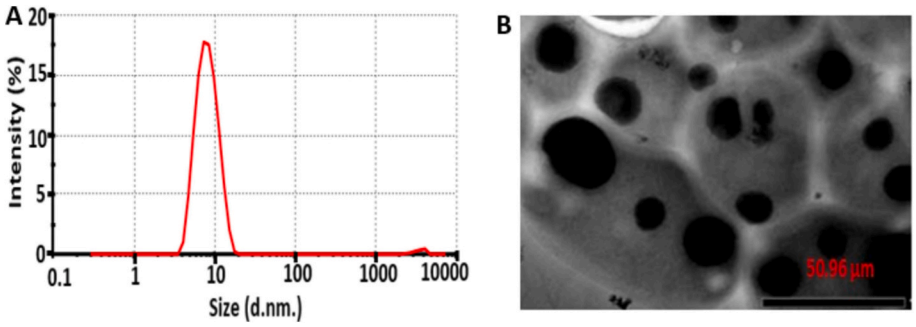

Fig. 5. Surface morphology and size distribution of TB-CQDs in the presence of acrylamide (A) Particle size Analysis (B) HR-TEM. Data are presented as means ± SD (n = 3).

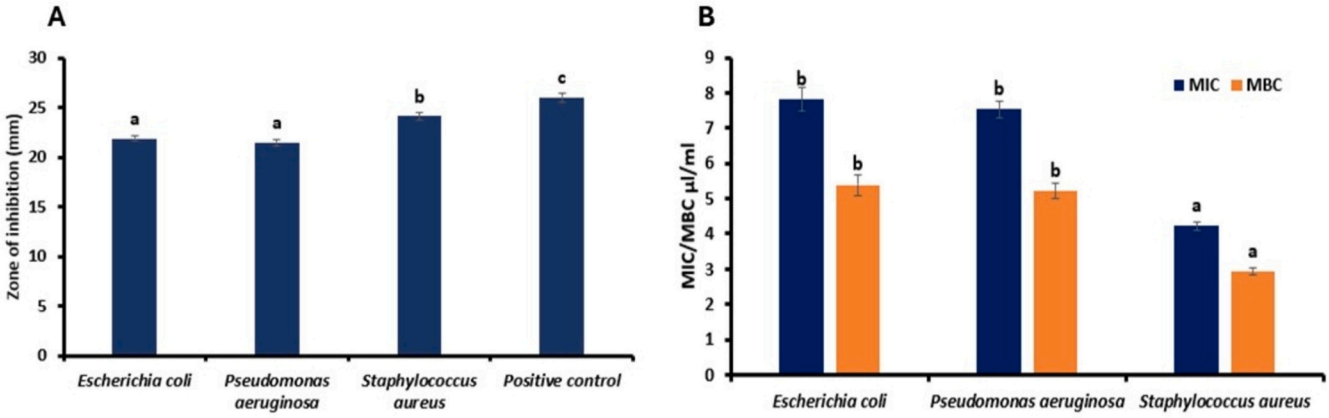

Fig. 6. Antimicrobial efficacy of TB-CQDs against *Escherichia coli, Pseudomonas aeruginosa, and Staphylococcus aureus* (A) Zone of inhibition, and (B) MIC and MBC. The results were expressed as mean ± standard deviation of >3 independent replicates. The mean value with different lowercase (a-c) alphabets within the column represents significantly different values from each other which was analyzed based on the ANOVA (analysis of variance) and post hoc test.

higher zone of inhibition against the gram-positive *Staphylococcus aureus* (24.12 ± 0.38 mm) relative to Gram-negative counterparts. The observed zones of inhibition for *Escherichia coli,* and *Pseudomonas aeruginosa* were measured at 21.89 ± 0.26, and 21.45 ± 0.29, respectively. Additionally, Fig. 6B outlines the Minimum Inhibitory Concentration (MIC) and Minimum Bactericidal Concentration (MBC) data of TBW-CQDs against each bacterial strain. The determined MIC values *Escherichia coli, Pseudomonas aeruginosa,* and, *Staphylococcus aureus*, were recorded as 7.82 ± 0.35, 7.53 ± 0.23, and 4.23 ± 0.12, µL/mL, respectively. Also, the observed MBC values were 5.38 ± 0.31, 5.21 ± 0.21, and 2.93 ± 0.09 µL/mL, respectively. The inhibitory efficacy of TBW-CQDs on microbial growth is attributed to the presence of diverse functional groups within the carbon dots, potentially interfering with cellular enzymatic processes and impeding cellular proliferation. The antimicrobial mode of action of TBW-CQDs is reported to involve reactive oxygen species generation, electrostatic interactions, and susceptibility to light exposure. FTIR and EDS (Energy dispersive X-ray spectroscopy) identified reactive oxygen species ROS, including carboxyl groups and hydroxyl radicals. These species are responsible for showcasing antimicrobial effects. The presence of positively charged hydrogen elements on TBW-CQDs facilitates their adherence to negatively charged microbial surfaces, leading to membrane penetration and subsequent microbial demise. These results are similarity trend with (Nguyen et al., 2024) highlighting the antimicrobial efficacy of orange juice-derived CQDs against *Escherichia coli* by recording MIC of 1 ppm.

3.9. Photocatalytic dye degradation

The UV spectrums of methylene blue and indigo carmine in the presence of TBW-CQDs under sunlight are given in Fig. 6. The results demonstrate a significant degradation of 91.62 % and 95.29 % of indigo carmine and methylene blue under 120 and 90 min, respectively.

In the beginning, there was no apparent removal observed. However, after 45 min, 51.96 % of methylene blue and 48.29 % of indigo carmine were degraded. Following this, the rate of degradation increased to 93.19 % after 90 min and 90.62 % after 120 min for methylene blue and indigo carmine, respectively. Fig. 7 demonstrates the reduction efficiency of both dyes by TBW-CQDs under natural sunlight. Similar results have been highlighted by Edakkaparamban et al. (2023), who fabricated CQDs from coconut husk and utilized them to degrade methylene blue up to 94 % within 150 min.

4. Conclusion

The present work developed sustainable and novel fluorescence tea-derived carbon quantum dots by utilizing the hydrothermal method for the determination of acrylamide in drinking water samples and dye degradation. The TBW-CQDs exhibit excellent stability and strong fluorescence properties. The particle size, chemical structure, and morphology of the TBW-CQDs were explored by utilizing advanced instruments such as a particle size analyzer, HR-TEM, AFM, FTIR, and DSC highlighting the fabrication of nanoparticles. The approach provides various advantages including economical, sensitive, biocompatible, waste utilization, and easy sample preparation. Despite several advantages, the developed method determined a broad acrylamide with a remarkably low LOD of 0.35376 ppm. Moreover, this green fluorescence approach displayed exceptional accuracy, precision, and repeatability. Furthermore, when these results were compared to the HPLC technique, the TBW-CQD-based sensor provided sensitive and similar results. Our

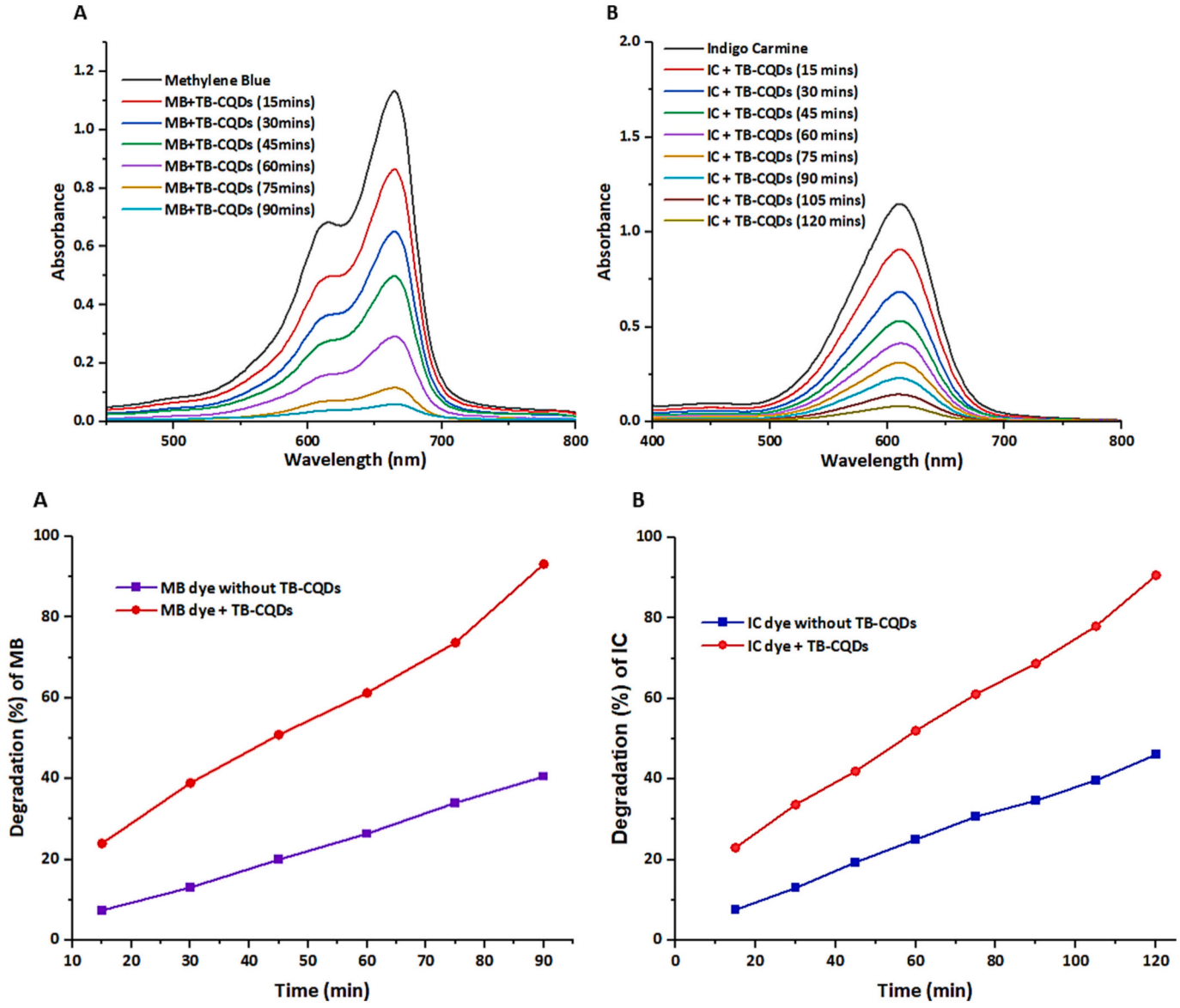

Fig. 7. (a) Photocatalytic Dye Degradation by TB-CQDs (A) UV–visible spectra of Methylene blue dye after 90 min. (B) UV–visible spectra of Indigo carmine dye after 120 min. Data are presented as means ± SD (n = 3). (For interpretation of the references to color in this figure legend, the reader is referred to the web version of this article.)

(b) Photocatalytic Dye Degradation by TB-CQDs (A) Degradation (%) of Methylene blue (B) Degradation (%) of Indigo carmine. Data are presented as means ± SD (n = 3). (For interpretation of the references to color in this figure legend, the reader is referred to the web version of this article.)

work effectively employed TBW-CQDs for the photocatalytic degradation of 90.12 % indigo carmine and 95.26 % methylene blue under sunlight within 120 and 90 min, demonstrating their promising potential in wastewater treatment applications. These TBW-CQDs hold significant antimicrobial potential against *Escherichia coli, Pseudomonas aeruginosa,* and, *Staphylococcus aureus* and emerge as promising techniques for practical application in drug delivery, gene therapy, bioimaging, and biosensors.

CRediT authorship contribution statement

Nikhil Sharma: Writing – original draft, Methodology, Investigation, Formal analysis, Data curation. **Sweezee Thakur:** Writing – review & editing, Methodology, Formal analysis. **Aarti Bains:** Writing – review & editing, Methodology, Formal analysis. **Gulden Goksen:** Formal analysis, Data curation, Methodology, Writing - review & editing. **Nemat Ali:** Writing – review & editing, Methodology, Formal analysis. **Mushtaq Ahmad Ansari:** Writing – review & editing, Methodology. **Anna Kopsacheili:** Writing – review & editing, Methodology. **Charalampos Proestos:** Writing – review & editing, Resources, Methodology, Funding acquisition. **Prince Chawla:** Writing – review & editing, Validation, Supervision, Software, Resources, Project administration, Methodology, Investigation, Conceptualization.

Declaration of competing interest

The authors declare that they have no known competing financial interests or personal relationships that could have appeared to influence the work reported in this article.

Acknowledgment

The authors acknowledge and extend their appreciation to the Researchers Supporting Project Number (RSPD2025R940), King Saud University, Riyadh, Saudi Arabia for supporting this study. We thank the National and Kapodistrian University of Athens, Special Account for Research Grants, No. 14053.

Data availability

Data will be made available on request.

References

Abu-Melha, S. (2024). Metal-doped carbon quantum dots for catalytic discoloration of methylene blue in day light. *Journal of photochemistry and photobiology. A Chemistry, 447*(115233), Article 115233. https://doi.org/10.1016/j.jphotochem.2023.115233

Agbasi, J. C., Ezugwu, A. L., Omeka, M. E., Ucheana, I. A., Aralu, C. C., Abugu, H. O., & Egbueri, J. C. (2024). More about making profits or providing safe drinking water? A state-of-the-art review on sachet water contamination in Nigeria. *Journal of Environmental Science and Health. Part C, Toxicology and Carcinogenesis*, 1–43. https://doi.org/10.1080/26896583.2024.2319009

Alamdari, N. G., Almasi, H., Moradi, M., & Akhgari, M. (2023). Characterization of carbon quantum dots synthesized from vinasse and date seeds as agro-industrial wastes. *Waste and Biomass Valorization, 14*(11), 3689–3703. https://doi.org/10.1007/s12649-023-02087-7

Allen, R. C. (1978). Applications of polyacrylamide gel electrophoresis and polyacrylamide gel isoelectric focusing in clinical chemistry. *Journal of Chromatography, 146*(1), 1–32. https://doi.org/10.1016/s0378-4347(00)81286-4

Anpalagan, K., Yin, H., Cole, I., Zhang, T., & Lai, D. T. H. (2024). Quantum yield enhancement of carbon quantum dots using chemical-free precursors for sensing Cr (VI) ions. *Inorganics, 12*(4), 96. https://doi.org/10.3390/inorganics12040096

Atchudan, R., Edison, J. I., & T. N., Shanmugam, M., Perumal, S., Somanathan, T., & Lee, Y. R.. (2021). Sustainable synthesis of carbon quantum dots from banana peel waste using hydrothermal process for in vivo bioimaging. *Physica. E, Low-Dimensional Systems & Nanostructures, 126*(114417), Article 114417. https://doi.org/10.1016/j.physe.2020.114417

Aygun, A., Cobas, I., Tiri, R. N. E., & Sen, F. (2024). Hydrothermal synthesis of B, S, and N-doped carbon quantum dots for colorimetric sensing of heavy metal ions. *RSC Advances, 14*(16), 10814–10825. https://doi.org/10.1039/d4ra00397g

Baslak, C., Demirel, S., Kocyigit, A., Erdal, M. O., & Yıldırım, M. (2023). Electrolyte performance of green synthesized carbon quantum dots from fermented tea for high-speed capacitors. *Diamond and Related Materials, 139*(110275), Article 110275. https://doi.org/10.1016/j.diamond.2023.110275

Casanova, L., Beldjilali, S. A., Bilge, G., Sezer, B., Motto-Ros, V., Pelascini, F., … Hermann, J. (2023). Evaluation of limits of detection in laser-induced breakdown spectroscopy: Demonstration for food. *Spectrochimica Acta. Part B: Atomic Spectroscopy, 207*(106760), Article 106760. https://doi.org/10.1016/j.sab.2023.106760

Dilebo, T., Feyissa, T., Asfaw, Z., & Zewdu, A. (2023). Analysis of proximate composition, mineral contents, and anti-nutritional factors of enset (Ensete ventricosum) landraces commonly used for amicho preparation in Hadiya zone, southern Ethiopia: Implications for food security and mineral bioavailability. *Journal of Agriculture and Food Research, 14*(100771), Article 100771. https://doi.org/10.1016/j.jafr.2023.100771

Edakkaparamban, S., Kitamura, M., Ide, Y., Umemura, K., & Ishizawa, A. (2023). Photocatalytic degradation study of methylene blue using carbon quantum dots synthesized from coconut husk. *Materials Letters, 345*(134508), Article 134508. https://doi.org/10.1016/j.matlet.2023.134508

Fan, M., Xu, X., Lang, W., Wang, W., Wang, X., Xin, A., Zhou, F., Ding, Z., Ye, X., & Zhu, B. (2023). Toxicity, formation, contamination, determination and mitigation of acrylamide in thermally processed plant-based foods and herbal medicines: A review. *Ecotoxicology and Environmental Safety, 260*(115059), Article 115059. https://doi.org/10.1016/j.ecoenv.2023.115059

Farouk, S. M., Gad, F. A., Almeer, R., Abdel-Daim, M. M., & Emam, M. A. (2021). Exploring the possible neuroprotective and antioxidant potency of lycopene against acrylamide-induced neurotoxicity in rats' brain. *Biomedecine & Pharmacotherapie [Biomedicine & Pharmacotherapy], 138*(111458), Article 111458. https://doi.org/10.1016/j.biopha.2021.111458

Gupta, D., Singh, S., Soni, R., Gupte, S. S., Rathour, A., Shrivastava, S., & Shukla, S. (2023). Possible metabolic effect of acrylamide on biological system. *Food Safety and Health, 1*(2), 126–138. https://doi.org/10.1002/fsh3.12020

Gür, F., Cengiz, M., Gür, B., Cengiz, O., Sarıçiçek, O., & Ayhancı, A. (2023). Therapeutic role of boron on acrylamide-induced nephrotoxicity, cardiotoxicity, neurotoxicity, and testicular toxicity in rats: Effects on Nrf2/Keap-1 signaling pathway and oxidative stress. *Journal of Trace Elements in Medicine and Biology: Organ of the Society for Minerals and Trace Elements (GMS), 80*(127274), Article 127274. https://doi.org/10.1016/j.jtemb.2023.127274

Hu, X., Li, Y., Xu, Y., Gan, Z., Zou, X., Shi, J., Huang, X., Li, Z., & Li, Y. (2021). Green one-step synthesis of carbon quantum dots from orange peel for fluorescent detection of Escherichia coli in milk. *Food Chemistry, 339*(127775), Article 127775. https://doi.org/10.1016/j.foodchem.2020.127775

Inayat, A., Albalawi, K., Rehman, A.-U., Adnan, S., & A. Y., Saleh, E. A. M., Alamri, M. A., El-Zahhar, A. A., Haider, A., & Abbas, S. M.. (2023). Tunable synthesis of carbon quantum dots from the biomass of spent tea leaves as supercapacitor electrode. *Materials Today. Communications, 34*(105479), Article 105479. https://doi.org/10.1016/j.mtcomm.2023.105479

Irmania, N., Dehvari, K., Gedda, G., Tseng, P.-J., & Chang, J.-Y. (2020). Manganese-doped green tea-derived carbon quantum dots as a targeted dual imaging and photodynamic therapy platform. *Journal of Biomedical Materials Research. Part B, Applied Biomaterials, 108*(4), 1616–1625. https://doi.org/10.1002/jbm.b.34508

John, B. K., Mathew, J., Sreekanth, E., & R., & Mathew, B.. (2024). Biomass derived carbon quantum dots as a versatile platform for fluorescent sensing, catalytic reduction, fluorescent ink and anticancer agents. *Materials Today Sustainability, 26*(100715), Article 100715. https://doi.org/10.1016/j.mtsust.2024.100715

Kalpana, R., Sakthi Vignesh, N., Vinothini, K., Rajan, M., Ashokkumar, B., Brindhadevi, K., Thuy Lan Chi, N., Pugazhendhi, A., & Varalakshmi, P. (2023). Carbon quantum dots (CQD) fabricated from Exiguobacterium sp. VK2 exopolysaccharide (EPS) using hydrothermal reaction and its biodiesel applications. *Fuel (London, England), 333*(126426), Article 126426. https://doi.org/10.1016/j.fuel.2022.126426

Kasinathan, K., Samayanan, S., Marimuthu, K., & Yim, J.-H. (2022). Green synthesis of multicolour fluorescence carbon quantum dots from sugarcane waste: Investigation of mercury (II) ion sensing, and bio-imaging applications. *Applied Surface Science, 601*(154266), Article 154266. https://doi.org/10.1016/j.apsusc.2022.154266

Kechagias, A., Lykos, C., Vassilios, K., Karabagias, S., Georgopoulos, V., Sakavitsi, A., … Giannakas, I. (2023). Development and characterization of N/S-carbon quantum dots by valorizing Greek crayfish food waste. *Applied Sciences, 13*(15).

Kuppusamy, P., Kim, S., Park, M., & Song, K.-D. (2024). Commercial wheat and oat flour derived fluorescent carbon quantum dots through sustainable hydrothermal synthesis and their biological activities. *ChemistrySelect, 9*(11). https://doi.org/10.1002/slct.202303994

Molaei, M. J. (2024). Synthesis and application of carbon quantum dots derived from carbon black in bioimaging. *Journal of Fluorescence, 34*(1), 213–226. https://doi.org/10.1007/s10895-023-03252-w

Mpili, P., Vicent, V., & Rweyemamu, L. (2024). Evaluation of the proximate composition, functional, and pasting properties of ichipipi maize flour. *Applied Food Research, 4*(1), Article 100408. https://doi.org/10.1016/j.afres.2024.100408

Nguyen, M. H., Le, A. T., Pham, V. D., Pham, H. M., Do, H. T., Le, D. T., … Nguyen, T. B. (2024). A comprehensive study on the antibacterial activities of carbon quantum dots derived from orange juice against Escherichia coli. *Applied Sciences (Basel, Switzerland), 14*(6), 2509. https://doi.org/10.3390/app14062509

Olugbuyi, A., Oyinloye, A., Araoye, K., & Ariseloye, O. (2024). Orange fleshed sweet potato-rice bran flour: Optimization, proximate and amino acid composition for dough meal production. *Journal of Agriculture and Food Research, 15*(100920), Article 100920. https://doi.org/10.1016/j.jafr.2023.100920

Osorio, L. L. D. R., Flórez-López, E., & Grande-Tovar, C. D. (2021). The potential of selected Agri-food loss and waste to contribute to a circular economy: Applications

in the food, cosmetic and pharmaceutical industries. *Molecules (Basel, Switzerland), 26*(2), 515. https://doi.org/10.3390/molecules26020515

Pandiyan, S., Arumugam, L., Srirengan, S. P., Pitchan, R., Sevugan, P., Kannan, K., … Gandhirajan, V. (2020). Biocompatible carbon quantum dots derived from sugarcane industrial wastes for effective nonlinear optical behavior and antimicrobial activity applications. *ACS Omega, 5*(47), 30363–30372. https://doi.org/10.1021/acsomega.0c03290

Pourmadadi, M., Tajiki, A., Abdouss, M., Beig Mohammadi, A., Kharaba, Z., Rahdar, A., & Díez-Pascual, A. M. (2024). Novel carbon quantum dots incorporated polyacrylic acid/polyethylene glycol pH-sensitive nanoplatform for drug delivery. *Inorganic Chemistry Communications, 159*(111814), Article 111814. https://doi.org/10.1016/j.inoche.2023.111814

Pushparaj, K., Liu, W.-C., Meyyazhagan, A., Orlacchio, A., Pappusamy, M., Vadivalagan, C., & Asirvatham, A. (2022). Nano-from nature to nurture: A comprehensive review on facets, trends, perspectives and sustainability of nanotechnology in the food sector. *Energy, 240*.

Rajput, S. D., Pandey, N., & Sahu, K. (2024). A comprehensive report on valorization of waste to single cell protein: Strategies, challenges, and future prospects. *Environmental Science and Pollution Research International, 31*(18), 26378–26414. https://doi.org/10.1007/s11356-024-33004-7

Salman, B. I. (2024). An innovative selective fluorescence sensor for quantification of hazardous food colorant Allura red in beverages using nitrogen-doped carbon quantum dots. *Journal of Fluorescence, 34*(2), 599–608. https://doi.org/10.1007/s10895-023-03303-2

Sandeep Kumar Jain, R., Meghana, P., Prashanth, N., Santhosh Kumar, J. U., Satyanarayan, N. D., Sharath, R., … Kumaraswamy, H. M. (2023). Phenolic fingerprint, proximate analysis and nutraceutical effects of Garcinia talbotii, an under-utilized functional food endemic to Western Ghats. *Food Bioscience, 54*(102894), Article 102894. https://doi.org/10.1016/j.fbio.2023.102894

Sistani, S., & Shekarchizadeh, H. (2021). Fabrication of fluorescence sensor based on molecularly imprinted polymer on amine-modified carbon quantum dots for fast and highly sensitive and selective detection of tannic acid in food samples. *Analytica Chimica Acta, 1186*(339122), Article 339122. https://doi.org/10.1016/j.aca.2021.339122

Taloor, A., Kumar, S., Sharma, S., Suryakiran, R., & Sharma, M. (2024). A groundwater contamination and health risk assessment in Indian subcontinent: A geospatial approach. *Current Opinion in Environmental Science & Health, 39, 100555.*

Tepe, Y. (2024). Acrylamide in surface and drinking water. In *Acrylamide in food* (pp. 285–305). Elsevier. https://doi.org/10.1016/b978-0-323-99119-3.00011-4.

Thakur, S., Bains, A., Inbaraj, B. S., Sridhar, K., Kumar, A., Yaqoob, M., … Sharma, M. (2024). Synthesis of carbon quantum dots from waste Phaseolus vulgaris for the development of a fluorescence sensing probe to detect plasticizer in cookies. *Process Safety and Environmental Protection : Transactions of the Institution of Chemical Engineers, Part B, 184*, 650–659. https://doi.org/10.1016/j.psep.2024.02.005

Thakur, S., Bains, A., Kumar, A., Goksen, G., Yaqoob, M., Parvez, M. K., … Chawla, P. (2024). Biomass valorization of liquid whey into carbon quantum dots via hydrothermal process for food pathogenic bactericidal activity and photocatalytic degradation of brilliant red dye. *Food Bioscience, 58*(103764), Article 103764. https://doi.org/10.1016/j.fbio.2024.103764

Tungare, K., Bhori, M., Racherla, K. S., & Sawant, S. (2020). Synthesis, characterization and biocompatibility studies of carbon quantum dots from Phoenix dactylifera. *3. Biotech, 10*(12), 540. https://doi.org/10.1007/s13205-020-02518-5

Vijeata, A., Chaudhary, G. R., & Chaudhary, S. (2024). Lateral flow assemblies and allied application of carbon quantum dots derived from cigarette tobacco in biosensing, anticounterfeiting and fluorescent films: Theoretical and experimental overview. *Chemosphere, 355*, Article 141812. https://doi.org/10.1016/j.chemosphere.2024.141812

Vyas, T., & Joshi, A. (2024). Chemical sensor thin film-based carbon quantum dots (CQDs) for the detection of heavy metal count in various water matrices. *The Analyst, 149*(4), 1297–1309. https://doi.org/10.1039/d3an01571h

Wei, Q., Liu, T., Pu, H., & Sun, D.-W. (2020). Determination of acrylamide in food products based on the fluorescence enhancement induced by distance increase between functionalized carbon quantum dots. *Talanta, 218*(121152), Article 121152. https://doi.org/10.1016/j.talanta.2020.121152

Wei, Q., Zhang, P., Liu, T., Pu, H., & Sun, D.-W. (2021). A fluorescence biosensor based on single-stranded DNA and carbon quantum dots for acrylamide detection. *Food Chemistry, 356*(129668), Article 129668. https://doi.org/10.1016/j.foodchem.2021.129668

Yan, F., Wang, L., Zhao, L., Wang, C., Lu, Q., & Liu, R. (2023). Acrylamide in food: Occurrence, metabolism, molecular toxicity mechanism and detoxification by phytochemicals. *Food and Chemical Toxicology: An International Journal Published for the British Industrial Biological Research Association, 175*(113696), Article 113696. https://doi.org/10.1016/j.fct.2023.113696

Yazıcı, E., Bodur, S., Erarpat, S., Arslan, U. E., & Bakırdere, S. (2023). Assessment of external calibration, internal standard calibration and quadruple isotope dilution strategies for the determination of acrylamide in wastewater samples after LC-MS/MS quantification. *Microchemical Journal, Devoted to the Application of Microtechniques in All Branches of Science, 190*(108741), Article 108741. https://doi.org/10.1016/j.microc.2023.108741

Zafar, S. H., Umair, M., & Akhtar, M. (2023). Nutritional evaluation, proximate and chemical composition of mungbean varieties/cultivars pertaining to food quality characterization. *Food Chemistry Advances, 2*(100160), Article 100160. https://doi.org/10.1016/j.focha.2022.100160

Zhang, S., Mao, Y., Sun, J., Song, T., Song, Z., Zhao, X., & Wang, W. (2023). One-pot solvothermal preparation of triple-emission N, cl doped carbon quantum dots from waste traditional Chinese medicines as a fluorescent sensor for sensing water and Cr (VI). *Colloids and Surfaces. A, Physicochemical and Engineering Aspects, 669*(131471), Article 131471. https://doi.org/10.1016/j.colsurfa.2023.131471

Zhong, Y., Zhang, X., Wang, Y., Zhang, X., & Wang, X. (2023). Carbon quantum dots from tea enhance z-type BiOBr/C3N4 heterojunctions for RhB degradation: Catalytic effect, mechanisms, and intermediates. *Applied Surface Science, 639*(158254), Article 158254. https://doi.org/10.1016/j.apsusc.2023.158254

Zhu, X., Zhou, Y., Yan, S., Qian, S., Wang, Y., Ju, E., & Zhang, C. (2024). Herbal medicine-inspired carbon quantum dots with antibiosis and hemostasis effects for promoting wound healing. *ACS Applied Materials & Interfaces, 16*(7), 8527–8537. https://doi.org/10.1021/acsami.3c18418